International Journal of Adhesion and Adhesives 82 (2018) 72–78

Contents lists available at ScienceDirect

International Journal of Adhesion and Adhesives

journal homepage: www.elsevier.com/locate/ijadhadh

Key parameters of biomimetic patterned surface for wet adhesion

Jun Xie, Meng Li, Qingwen Dai, Wei Huang, Xiaolei Wang*

College of Mechanical and Electrical Engineering, Nanjing University of Aeronautics and Astronautics, Nanjing 210016, People's Republic of China

ARTICLE INFO

Keywords:
CPUE
Coupling factors
Surface texture
Wet adhesion

ABSTRACT

Inspired by the polygonal arrays on the toe pads of tree frogs and newts, micro hexagonal pillars were fabricated on a cast polyurethane elastomer (CPUE) surface so that a network of interconnected channels was formed. To investigate the effect of channel sizes, adhesion experiments were carried out with a flat polymethyl methacrylate (PMMA) probe and the patterned surface of CPUE samples under wet conditions. It was found that single factors alone, such as channel width (*W*), length (*L*), and height (*H*) have a slight effect on wet adhesion force. Comparatively, the values of width-to-length (*W/L*), height-to-length (*H/L*), and height-to-width (*H/W*) determine the wet adhesion force significantly. Actually, the wet adhesion force is reduced with increasing *W/L* values. Furthermore, optimal ranges of *H/L* and *H/W* values clearly enhance the wet adhesion force, even considering the reduction with the increasing *W/L* values.

1. Introduction

The strong adhesion capability that some animals display has been an important area of research over the past decades. With such remarkable ability, some crawling animals can climb, attach to various surfaces, and hang upside down. A large number of studies have shown that this adhesion ability is closely related to the micro-patterns on their toe-pads.

Gecko is a typical animal that has been found to utilize van der Waals forces for dry adhesion [1,2]. These interaction forces are achieved by the direct contact of a hierarchical organization, which consists of millions of branched setae, each of them ending with thousands of spatula tips [3]. In addition to dry adhesion, wet adhesion is also an interesting ability for that amphibious animals exhibit. For example, tree frogs and newts can quickly climb and attach on wet, slippery rocks or leaves of plants. Observed by the naked eyes, their pads are flat and smooth. However, under a scanning electron microscope (SEM), they are patterned with hexagonal arrays of epithelial cells separated by mucus-filled channels [4–6]. Unlike dry adhesion, a thin fluid layer always lies between the substrate and toe pads in wet adhesion, and the adhesion force is mainly attributed to the combined effect of capillary and Steffen adhesion [5,7].

It has been proposed that the excess fluid has to be squeezed out of the contact zone quickly, facilitated by the micro-structure of the tree frogs' toe pads, to prevent hydrodynamic lubrication and achieve tight adhesion [7,8]. Drotlef et al. made different structured polydimethylsiloxane (PDMS) surfaces and proved that the wet adhesion force is dependent on the presence of the microstructure and its geometrical characteristics [9]. A network of interconnected channels, with a specific channel depth, width, and post diameter, results in significant reduction in hydrodynamic repulsion, compared to smooth surfaces [10]. Iturri et al. showed that elongated PDMS hexagonal patterns with an optimum pillar height increase friction forces, considering the deformability and edge density of pillars [11]. Huang et al. found that a pillar-patterned surface with high area density can maintain high friction at high sliding speed, which is different from micro-dimple patterned surfaces [12,13]. According to these studies, the dimensional design of hexagonal pillars and interconnected channels is closely related to the friction force. Unfortunately, few studies have been conducted until now to explore whether the wet adhesion of bio-microstructured surfaces is related to the sizes of pillars or channels. In addition, the most commonly used elastic material in biomimetic adhesion tests is PDMS, which has approximately a 110 ° static contact angle of its surface, and it is a well-known hydrophobic surface, contrary to the hydrophilic surface of the pads of the aforementioned animals. Therefore, it is apparent that a comprehensive and systematic study of micro hexagonal pillars' geometry sizes is essential to find out their influence mechanisms of wet adhesion, and it would be significant for the biomimetic microstructure design for the machines such as active capsule endoscopy.

In this study, because the pad surface of frogs and newts is hydrophilic, a new hydrophilic elastic material, cast polyurethane elastomer (CPUE), was used. Furthermore, taking into account the geometrical sizes of the microstructures, hexagonal pillars with interconnected

* Corresponding author.
E-mail address: wxl@nuaa.edu.cn (X. Wang).

https://doi.org/10.1016/j.ijadhadh.2018.01.004
Accepted 27 December 2017
Available online 04 January 2018

channels of different parameters were designed, and face-to-face adhesion experiments were conducted in the presence of water.

2. Experimental section

2.1. CPUE - elastic material with hydrophilic surface

The Hei-Cast 8400 CPUE, purchased from HEI CAST (Tokyo, Japan), was selected to prepare the patterned samples. The cured CPUE surface is hydrophilic, with 70 ° static contact angle approximately; thus, compared to a PDMS surface, it is closer to the wettability of biological pads.

Hei-Cast 8400 is a typical casting material, which includes the component A (polymer polyol), B (polyisocyanate) and D (heterocyclic diol, as chain extender). The low viscosity of the A, B, and D mixture promises a fine flowing property and exact shape replication. Once the mixture is cured, the sample is highly elastic and hard to tear. By controlling the content of D, the Shore hardness can be adjusted from 10 HA to 90 HA and the Elastic modulus can vary in the range of 0.36 MPa to 5.09 MPa.

In this study, the mass ratio of A, B, and D was set to 100:100:150 and the mixture was cured under 60 °C for 90 min. The Shore hardness of the samples is about 50 HA and the Elastic modulus is approximately 1.56 MPa.

2.2. Fabrication of textures by two-stage transfer process

Usually, the casting-material mixture can be directly poured on a surface of SU-8 2075 photoresist (a series of negative epoxy resists, provided by Microchem, USA) patterned by a UV-LIGA (ultraviolet light-lithographie, galvanoformung and abformung) process in order to transfer the textures to the samples. However, because of the high surface energy of the CPUE, the bonding strength between the CPUE samples and wafers is too large to keep the SU-8 patterned surface on the wafers without damage.

Thus, in this paper, a two-stage transfer process was adopted to make the CPUE samples. The specific process is shown in Fig. 1, which includes three steps:

(a) Preparation: Hexagonal pillars of SU-8 photoresist were primarily made on the glass wafers by UV-LIGA technology. The required conditions, such as spin speed and exposure energy, were optimized to manufacture the specific patterns.
(b) First-stage of the pattern transfer process to make PDMS negative mold: PDMS is selected as the negative mold material because of its lower surface energy, so that the negative mold can be stripped from the glass wafers easily without damaging the photoresist pattern.
(c) Second-stage of the pattern transfer to make CPUE samples: The mixture of CPUE was well stirred, casted to negative mode, degassed in vacuum condition and cured under 60 °C for 90 min to obtain the micro-patterned samples.

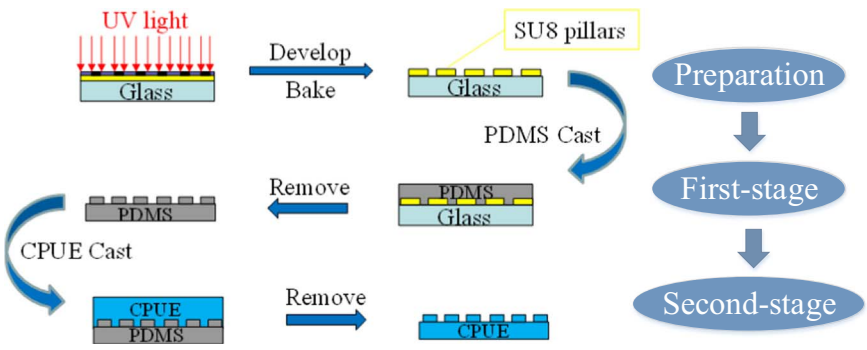

Fig. 1. Schematic diagram of two-stage transfer process.

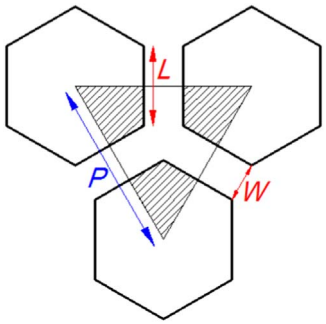

Fig. 2. Arrangement of hexagonal patterns. L is channel length, W is channel width and P is the center distance between two adjacent hexagons.

2.3. Pattern design of CPUE samples

The shape and distribution of the microstructures, shown in Fig. 2, were designed inspired by the textures of amphibian pads. Considering the real scale of the microstructures on amphibian toe-pads, SU-8 photoresist resolution, and manufacturing accuracy, different parameters of channel length, width, and height were chosen, as listed in Table 1.

The area density of hexagonal pillars can be defined as the ratio of hexagonal pillars area over the whole sample area. The area density of pillars (r_p) and the area density of channels (r_c) were calculated as follows, respectively:

$$r_p = 3L^2/P^2 \tag{1}$$

$$r_c = 1-3L^2/P^2 = 1-3/\left(\sqrt{3} + \frac{W}{L}\right)^2 \tag{2}$$

Fig. 3 shows three different patterned surfaces of the CPUE samples. The left image of each surface is the topography obtained by white light interferometer (Bruker, Germany), and the right image is the upper surface morphology observed by digital microscope (Keyence, Japan).

2.4. Adhesion measurements

Adhesion measurements were conducted with a self-made adhesion and friction tester [14], as shown in Fig. 4. The testing sample was brought into contact with the probe in a precise position by a piezo stage and two step motors. Wet adhesion tests were carried out with 2 μL of deionized water between the PMMA probe and CPUE samples. Both the probe and samples were of a cuboid shape with dimensions of 5 × 5 × 2 mm and 8 × 8 × 3 mm, respectively. Moreover, the 8 × 8 mm surface of the samples was in contact with the 5 × 5 mm surface of the probe, and thus, the contact area was 25 mm^2. There were 30 kinds of samples with different parameters, and each kind of sample had 8 specimens. In total, 240 specimens were tested in the adhesion measurements.

During the contact process, the contact condition was observed by

Table 1
Specific length, width, and height of channels.

Channel length L (μ m)	Channel width W (μ m)						Channel height H (μ m)
	r_c^*= 30%	r_c= 40%	r_c= 50%	r_c= 60%	r_c= 70%	r_c= 80%	
40	13.53	20.16	28.70	40.26	57.21	85.63	75
75	25.36	37.80	53.81	75.49	107.27	160.57	75
100	33.81	50.40	71.74	100.66	143.02	214.36	45,75,105

$^*r_c$ is the area density of micro-channels.

microscopes, and the deflection of the cantilever beam was continuously measured by a laser interferometer; thus, the contacting forces could be calculated by the cantilever deflection.

Roshan and Jayne showed that the wet adhesion force is related to the contact area, volume of liquid, preload, and speed of approach on adhesion [15]. Therefore, in this study, these factors were kept consistent in the adhesion measurements.

To describe the adhesion test in detail, a recorded force-to-position curve is shown in Fig. 5. First, the CPUE samples were driven to the target X-Z positions by the two step motors followed by the piezo stage. During the approaching process in the Z direction, a liquid bridge was presented, and the force between the probe and sample was increased to the preload under the iterative move of the piezo stage in nano steps. After the approach, there was a 5 s pause at this position to achieve stability of the system. Then, the CPUE sample was slowly retracted from the probe by the piezo stage, later followed by the Z step motor. The recorded force would reach the maximum during the retraction process and this value is called the maximum wet adhesion force. Once the liquid meniscus between the sample and probe was broken off, the adhesion tests could be stopped manually.

Notably, Kroner et al. indicated that the angle between two contact flats has significant effect on the adhesion force, and even a small angle will lead to a sharp force decrease [16]. Thus, in order to measure the maximum adhesion force accurately, it is necessary to ensure the relative parallelism between the two samples, as far as possible. In these tests, the complete contact between the probe and samples was achieved by simultaneously adjusting the horizontality of the probe and

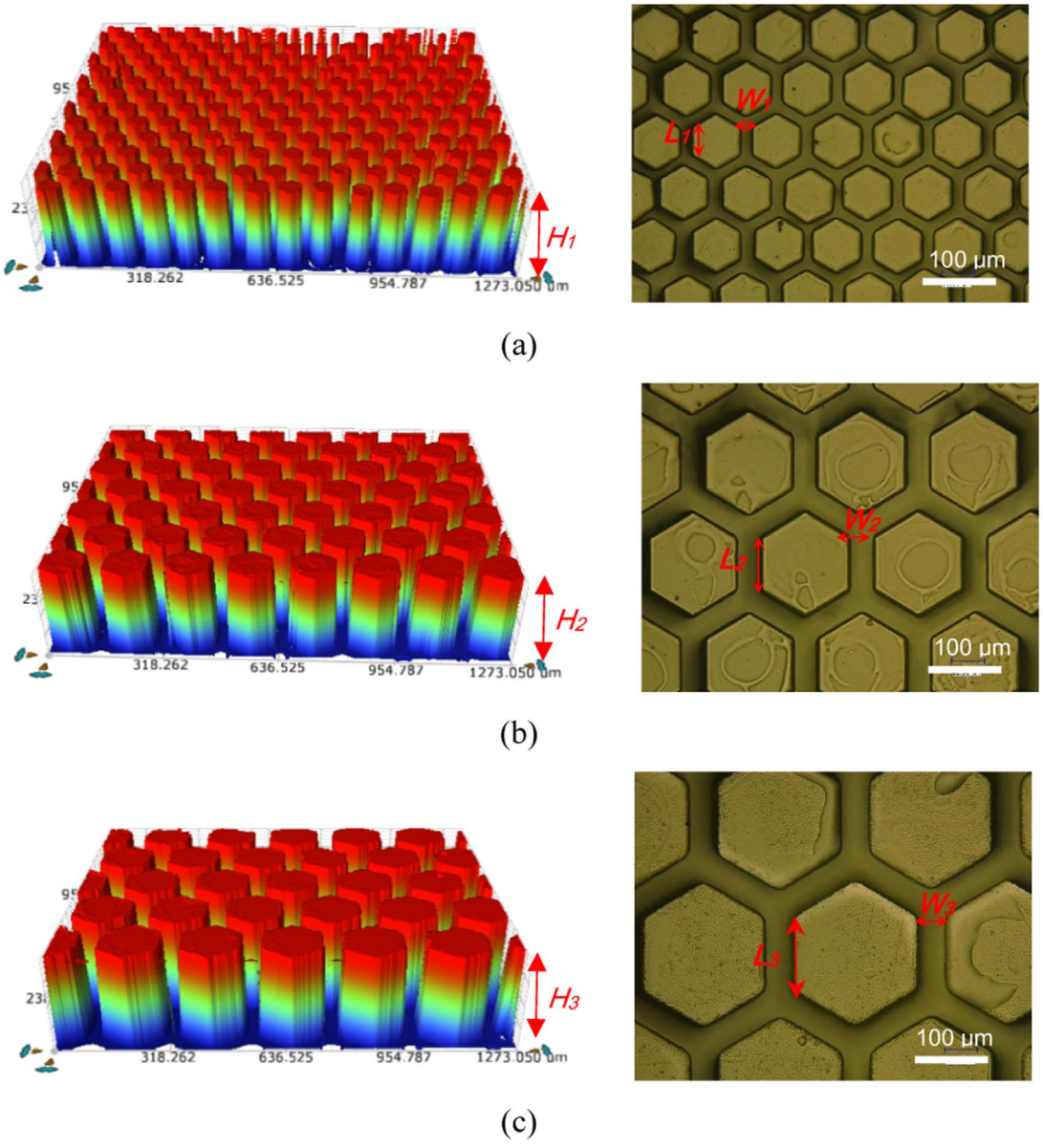

Fig. 3. Topography and microscope images of CPUE specimens used in the study with different parameters: (a) L_1 = 40 μm, W_1 = 20.16 μm, H_1 = 75 μm, (b) L_2 = 75 μm, W_2 = 37.80 μm, H_2 = 75 μm, (c) L_3 = 100 μm, W_3 = 50.40 μm, H_3 = 75 μm.

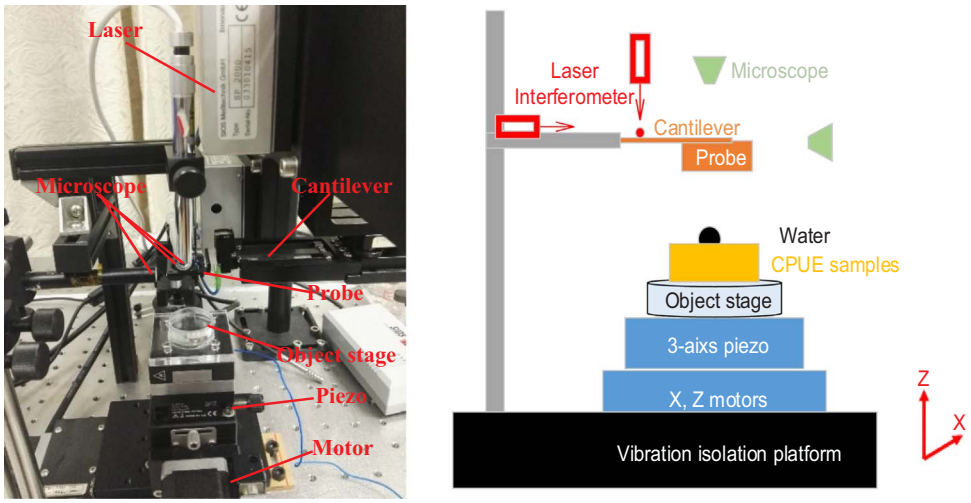

Fig. 4. Setup of adhesion and friction tester.

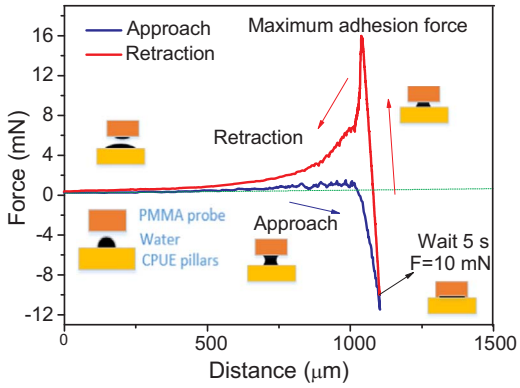

Fig. 5. Force-distance curve recorded with flat and microstructured (L = 100 μm, W = 71.74 μm, H = 75 μm) surfaces in the presence of 2 μL water.

sample surfaces. At the same time, aiming at objectivity and accuracy of the recorded data, eight standard measurements against the flat probe were performed in sequence with a fresh microstructured surface of the same pattern.

3. Results and discussion

In the following figures, each data point of adhesion force is the average of the eight measurements. Moreover, the error bars represent the standard deviation of these eight adhesion forces.

3.1. Effect of single factor on adhesion

3.1.1. Effect of channel width (W)

Fig. 6 is the evolution of adhesion force with channel width (W). Compared to the wet adhesion force, the dry adhesion force is much lower in each case. From Fig. 6(b) and (c), it can be observed that the increase channel width results in a decline of the wet adhesion force. In Fig. 6(a), there are two outstanding peaks where the wet adhesion force clearly increases.

It is well known that dry adhesion is a result of van der Walls Force, while in wet adhesion, there are additional forces, such as the capillary force [17]. Thus, wet adhesion force is much higher than dry adhesion force. When channel length (L) is fixed, the increase in channel width enlarges the distance between two adjacent hexagonal pillars. In that case, the amount of pillars is reduced, and thus, the actual contact area between the two surfaces is shrunk. Because of these changes, the wet adhesion force finally reduced [15,18,19].

3.1.2. Effect of channel length (L) and height (H)

The wet adhesion force of the flat probe and specimens also showed a dependence on channel length (L) and height (H), as displayed in Fig. 7.

Different from the effect of channel width on adhesion, adhesion force increases with channel length, as shown in Fig. 7(a). Although the channel area increases with its length, the density of channels declines. This is because the area of channels increases linearly with length, while the increase in pillars is quadratic, which means that the increase of channel area is smaller than that of pillars. Consequently, the actual contact area is increased.

From Fig. 7(b), it can be observed that adhesion force increases with increasing channel height when its value is less than 75 μm, and decreases if channel height is over 75 μm. Independently of the channel length, width, or height, 2 μL of water was sufficient to fill the interconnected channels, with 25 mm^2 of area, on the CPUE surface of the samples, and the excess water was extruded from the two contacting surfaces. When channel height was less than 75 μm, the volume of channels was enlarged with channel height (H). An increasing amount of water forms a liquid bridge [7,20] and the wet adhesion force is enhanced. However, with the further increase of H, the hexagonal pillars are taller and they are prone to cluster, leading to a decrease in actual contact area [11]. Therefore, the wet adhesion force finally decreases.

The above figures have shown the effect of channel width, length, and height on the maximum wet adhesion force, respectively. However, they are still unable to explain the peaks appeared in Fig. 6(a). Is it a coincidence? Or, perhaps, a single factor cannot fully explain how the channel sizes influence the wet adhesion force?

Hence, in the following paragraphs, coupling factors of channels were discussed, including width-to-length (W/L), height-to-length (H/L) and height-to-width (H/W).

3.2. Effect of coupling factors of channels on adhesion

3.2.1. Effect of width-to-length (W/L)

The value of W/L changes the features of channels on the contacting surface. Fig. 8 shows the effect of W/L on wet adhesion force. The adhesion force at low W/L ratios is much larger than that at high W/L ratios, as shown in the curves of L = 75 μm and L = 100 μm. It can be explained by Eq. (2) that the value of W/L directly determines the area density of channels (r_c), and r_c increases with an increasing W/L value. In general, the value of W/L influences the maximum adhesion force by changing the actual contact area between two flat surfaces, analogous to the influence mechanism of channel width and length. Accordingly, the effect of channel length and width on wet adhesion can be indicated

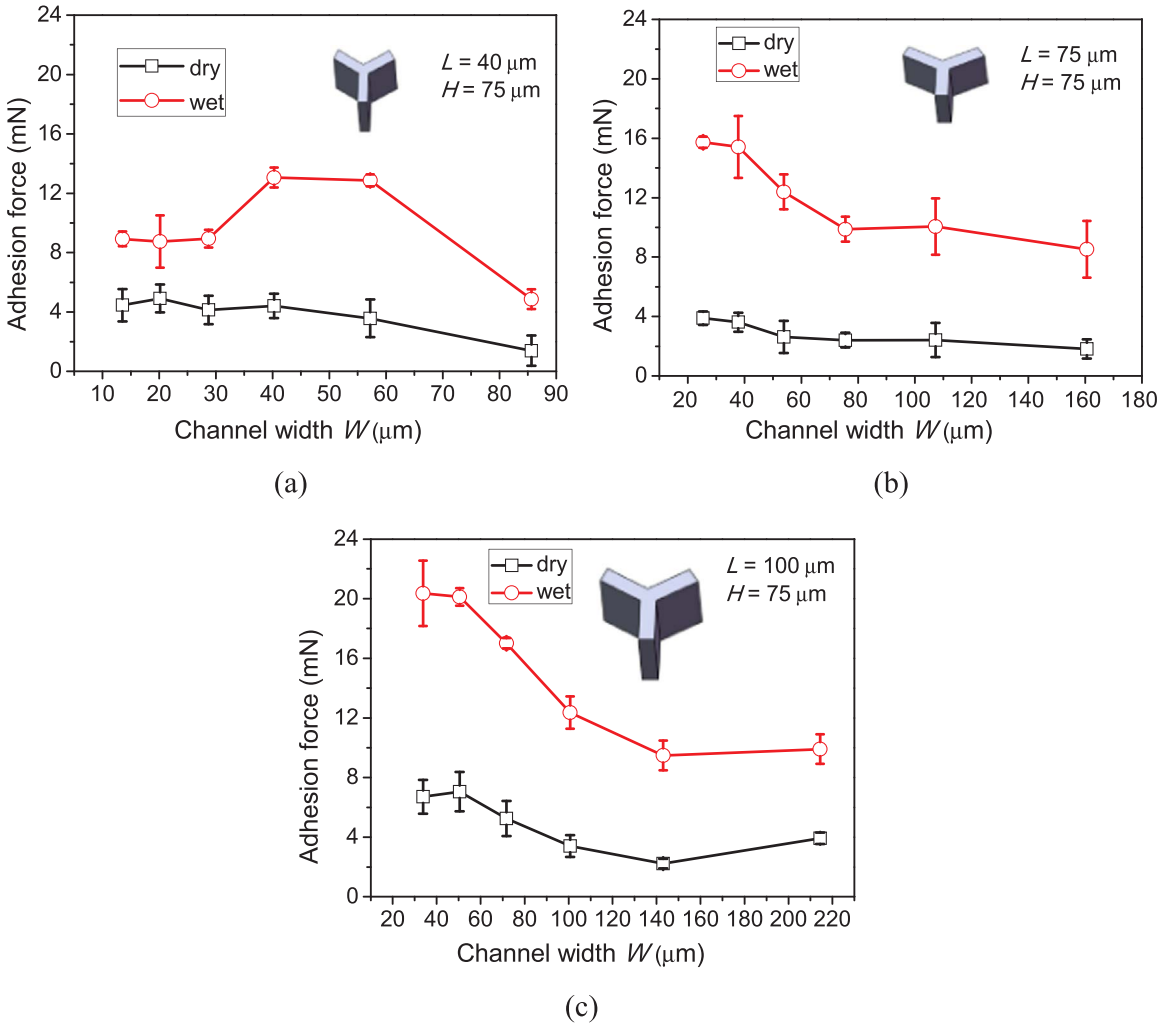

Fig. 6. Evolution of adhesion force with channel width (*W*). Specific parameters of three pictures are : (a) $L = 40$ μm, $H = 75$ μm, (b) $L = 75$ μm, $H = 75$ μm, (c) $L = 100$ μm, $H = 75$ μm.

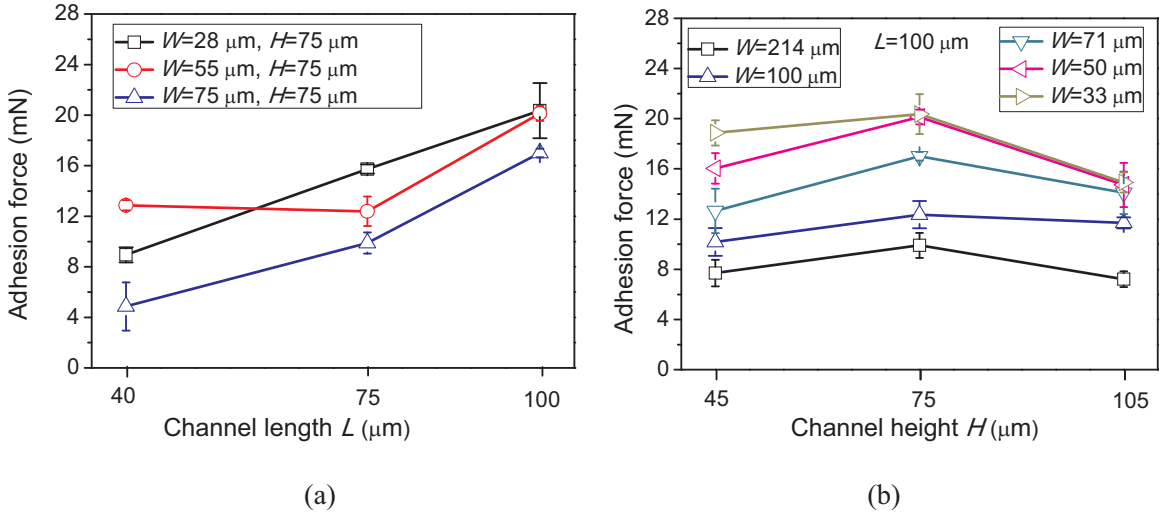

Fig. 7. Wet adhesion measurements performed with patterned surface of specimens under different (a) channel length *L* and (b) channel height *H*.

by the effect of *W/L* on wet adhesion.

However, based on the curve of $L = 40$ μm in Fig. 8, the wet adhesion force is not simply reduced with increasing *W/L*. It can be inferred that some other factors worked to evolve the wet adhesion force and led to the appearance of the peaks.

3.2.2. *Effect of height-to-length (H/L) and height-to-width (H/W)*

W/L reflects the geometrical characteristics of channels on the

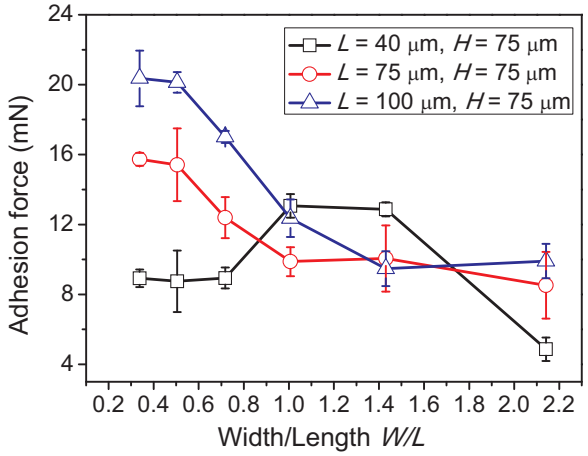

Fig. 8. Evolution of maximum wet adhesion force with width-to-length (*W/L*).

contacting surface, while *H/L* and *H/W* are the geometrical features of channels perpendicular to the contacting surface.

As shown in Fig. 9, the wet adhesion force increases with the rising values of *H/L* and *H/W* at first, and then decreases. In Fig. 9(a), the wet adhesion force increases with a value of *H/L* less than 0.75, and decreases above that value. In Fig. 9(b), the wet adhesion force increases with a value of *H/W* less than 1 and decreases with a value over 1.8. There are optimal ranges of the *H/L* and *H/W* values, in which the wet adhesion force could be enhanced greatly. The optimal range of *H/L* is from 0.7 to 0.9 and that of *H/W* is from 1.0 to 1.8, approximately, according to the curves in Fig. 9.

The evolution of the wet adhesion force in Fig. 9(a) is a result of the deformation of the hexagonal pillars. Different *H/L* values of channels cause different deformation modes of the pillars. When the value of *H/L* is low, the pillars are short and thick, and tend to be compressed. The actual contact area between the two surfaces increases slightly. If the *H/L* value is greater than the optimal range, the pillars are taller and thinner, and they can easily bend and cluster. The contact area decreases dramatically with further increase in *H/L* values [11].

The tendency in Fig. 9(b) is caused by the water flow behavior in the channels. When the distance between the two flat surfaces is small enough during the approach of the CPUE specimens to the probe, water forms a liquid meniscus [21]. With the decrease in distance between the two surfaces, water spreads around through the channels. The main orientation of water is the horizontal direction, as observed by the microscopes and depicted in Fig. 10(a). If the value of *H/W* is too large or small, the cross-sectional flow area will be very narrow. Huang et al. showed that because of the viscosity and surface tension of water, and the capillary effect, the resistance to a water flow is larger when the hole diameter is smaller [22]. Thus, it can be inferred that a narrow cross-sectional flow area largely hinders the channels from spreading the water away. Thus, the drainage performance of the channels is weaken and the water film thickness between the two surfaces is larger, contributing to a loss of wet contact area and, finally, a decrease in wet adhesion force.

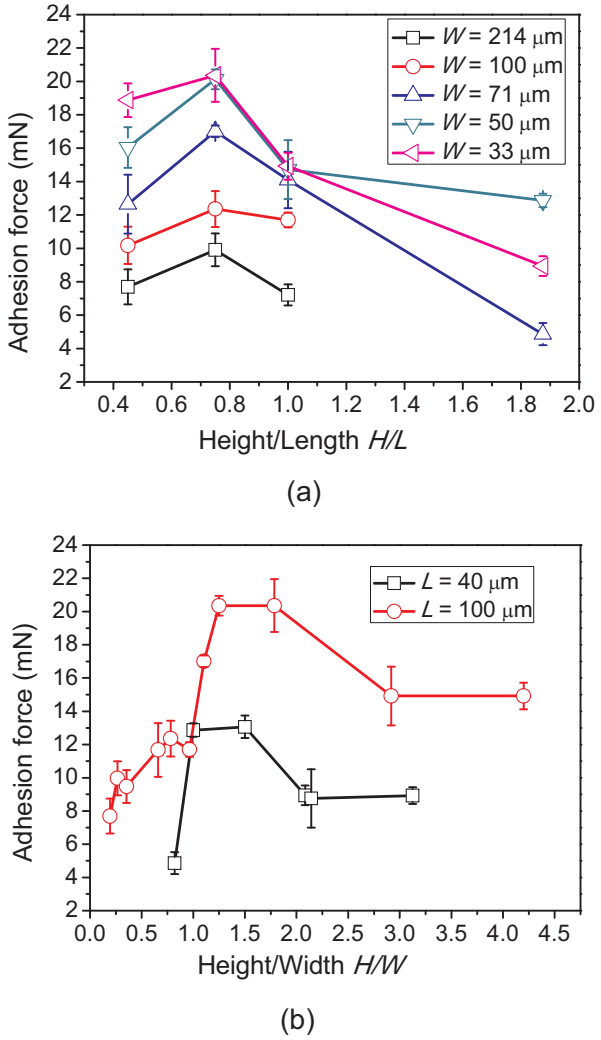

Fig. 9. Evolution of maximum wet adhesion force with: (a) height-to-length (*H/L*), (b) height-to-width (*H/W*) of channels.

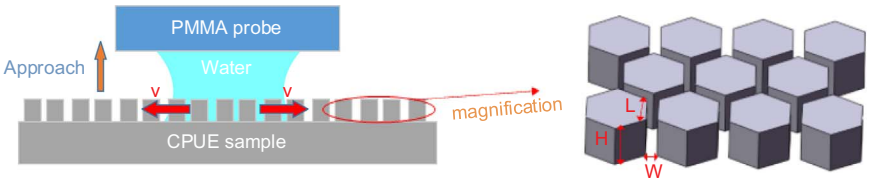

Fig. 10. Schematic diagram of water flow direction between two flat surfaces and the magnification of microstructures.

There are optimal ranges of H, H/L, and H/W. A different appropriate channel height will be chosen when the channel length and width are changed. However, because H/L and H/W are the combination of channel length, width, and height, the optimum ranges of H/L and H/W are suitable for hexagonal pillars of various sizes. The effect of H/L and H/W on adhesion is more representative than that of channel height.

It is now clear why peaks appeared in Fig. 6(a) and Fig. 8. It is because the H/W value of the first peak is approximately 1.3 and that of the second peak is about 1.6, and both are in the optimal range of H/W. Therefore, the wet adhesion force was greatly enhanced, despite a reduction with the increase in W/L values.

4. Conclusions

A large number of studies have shown that the amazing adhesion ability of the nature animals is closely related to the micro-patterns on their toe-pads. The comprehensive and systematic study to understand the mechanisms of the micro-patterns is significant for the biomimetic microstructure design for the machines such as active capsule endoscopy.

In this study, adhesion measurements were conducted with deionized water between two flat surfaces, the PMMA probe surface and the hydrophilic CPUE specimen surface featured with independent hexagonal pillars and interconnected channels. Various geometry factors were discussed, including the width (W), length (L), height (H), width-to-length (W/L), height-to-length (H/L), and height-to-width (H/W) of channels. The following conclusions can be drawn:

(1) Single factors (W, L, and H) have effect on adhesion force. However, they are not the only determinating factors that explain the variation in wet adhesion. Instead, the combination of factors, i.e., W/L, H/L, and H/W, can better determine the increases or decreases in wet adhesion force.
(2) The wet adhesion force decreases with an increase in the W/L value owing to the reduction in the actual contact area between the two flat surfaces.
(3) The optimal range of H/L is from 0.7 to 0.9, in which the wet adhesion force can be increased significantly. The values of H/L affect the wet adhesion force owing to the deformation of pillars.
(4) When the value of H/W is from 1 to 1.8, the wet adhesion force is increased owing to the improvement in the drainage capacity of the interconnected channels.

Acknowledgements

This research was supported by the National Nature Science Foundation of China (NSFC) (Grant No. 51675268) and the Fundamental Research Funds for the Central Universities (Grant NZ2016106).

References

[1] Autumn K, Peattie AM. Mechanisms of adhesion in geckos. Integr Comp Biol 2002;42(6):1081–90.
[2] Huber G, Mantz H, Spolenak R, et al. Evidence for capillarity contributions to gecko adhesion from single spatula nanomechanical measurements. Proc Natl Acad Sci USA 2005;102(45):16293–6.
[3] Huber G, Gorb SN, Spolenak R, et al. Resolving the nanoscale adhesion of individual gecko spatulae by atomic force microscopy. Biol Lett 2005;1(1):2–4.
[4] Federle W, Barnes WJ, Baumgartner W, et al. Wet but not slippery: boundary friction in tree frog adhesive toe pads. J R Soc Interface 2006;3(10):689–97.
[5] Wang S, LI M, HUANG W, et al. Sticking/climbing ability and morphology studies of the toe pads of Chinese fire belly newt. J Bionic Eng 2016;13(1):115–23.
[6] Barnes WJ, Oines C, Smith JM. Whole animal measurements of shear and adhesive forces in adult tree frogs: insights into underlying mechanisms of adhesion obtained from studying the effects of size and scale. J Comp Physiol A Neuroethol Sens Neural, Behav Physiol 2006;192(11):1179–91.
[7] Persson BNJ. Wet adhesion with application to tree frog adhesive toe pads and tires. J Phys: Condens Matter 2007;19(37):376110.
[8] Persson BNJ. Biological adhesion for locomotion basic principles. J Adhes Sci Technol 2007;21(12–13):1145–73.
[9] Drotlef D-M, Stepien L, Kappl M, et al. Insights into the adhesive mechanisms of tree frogs using artificial mimics. Adv Funct Mater 2013;23(9):1137–46.
[10] Gupta R, Frechette J. Measurement and scaling of hydrodynamic interactions in the presence of draining channels. Langmuir: ACS J Surf Colloids 2012;28(41):14703–12.
[11] Iturri J, Xue L, Kappl M, et al. Torrent frog-inspired adhesives: attachment to flooded surfaces. Adv Funct Mater 2015;25(10):1499–505.
[12] Huang W, Jiang L, Zhou C, et al. The lubricant retaining effect of micro-dimples on the sliding surface of PDMS. Tribol Int 2012;52:87–93.
[13] Huang W, Wang X. Biomimetic design of elastomer surface pattern for friction control under wet conditions. Bioinspir Biomim 2013;8(4):046001.
[14] Li M, Huang W, Wang X. Advanced adhesion and friction measurement system. Meas Sci Technol 2017;28(3):035601.
[15] Roshan R, Jayne DG, Liskiewicz T, et al. Effect of tribological factors on wet adhesion of a microstructured surface to peritoneal tissue. Acta Biomater 2011;7(11):4007–17.
[16] Kroner E, Paretkar DR, Mcmeeking RM, et al. Adhesion of flat and structured PDMS samples to spherical and flat probes: a comparative study. J Adhes 2011;87(5):447–65.
[17] Butt H-J, Barnes WJP, Del Campo A, et al. Capillary forces between soft, elastic spheres. Soft Matter 2010;6(23):5930.
[18] Kim H-Y, Mahadevan L. Capillary rise between elastic sheets. J Fluid Mech 2006;548(1):141.
[19] Navas CA, Endlein T, Barnes WJP, et al. Sticking under wet conditions: the remarkable attachment abilities of the torrent frog, staurois guttatus. PLoS One 2013;8(9):e73810.
[20] Yang C, Persson BNJ. Molecular dynamics study of contact mechanics contact area and interfacial separation from small to full contact. J Phys Condens Matter 2007.
[21] Kober M, Sahagun E, Garcia-mochales P, et al. Nanogeometry matters: unexpected decrease of capillary adhesion forces with increasing relative humidity. Small 2010;6(23):2725–30.
[22] An-liang H, Ping-chuan X, Jin-Jing C. The method to deal with the large error of Planck's constant error by the method of "inflection point method". Phys Exp Coll 2016;29(1).